A Chronically Implantable Neural Device for On-Demand Microdosing of Deep Brain Structures

by

Khalil B. Ramadi

B.S. Mechanical Engineering, The Pennsylvania State University (2014)

SUBMITTED TO THE DEPARTMENT OF MECHANICAL ENGINEERING IN PARTIAL FULFILLMENT OF THE REQUIREMENTS FOR THE DEGREE OF

MASTER OF SCIENCE IN MECHANICAL ENGINEERING
AT THE
MASSACHUSETTS INSTITUTE OF TECHNOLOGY

June 2016

Signature redacted

Signature of author.....
Department of Mechanical Engineering
May 19th, 2016

Signature redacted

Certified by.....
Michael J. Cima
Professor of Materials Science and Engineering
Thesis Supervisor

Signature redacted

Certified by.....
Robert S. Langer
Institute Professor
Thesis Reader

Signature redacted

Accepted by.....
Rohan Abeyaratne
Professor of Mechanical Engineering
Chairman, Department Committee on Graduate Students

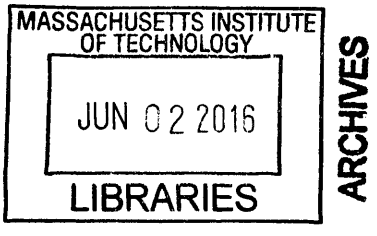

A Chronically Implantable Neural Device for On-Demand Microdosing of Deep Brain Structures

by

Khalil B. Ramadi

Submitted to the Department of Mechanical Engineering
On May 19, 2016
in Partial Fulfillment of the Requirements for the Degree of
Master of Science in Mechanical Engineering

Abstract

Chronic neuropsychiatric diseases are increasingly consuming a larger portion of healthcare costs, in part due to a lack of effective treatment techniques. Through research into the pathology of these diseases we now know that most of these disorders are due to a loss in synchrony in a specific neural network. Effective treatments must seek to attenuate these network dynamics to establish normal neural communication. However, current treatments lack the spatiotemporal resolution to target networks with such specificity. The 'Injectrode' device developed here is a dual-lumen brain probe that is chronically implanted with wirelessly programmable micropumps for drug delivery on-demand. We establish the functionality of the system for repeated delivery of down to a few nanoliters of drug on-demand *in vitro* and *in vivo*, and show its biocompatibility over a 2-month implantation. This provides the foundation for testing of the system in a disease model, as well as the incorporation of additional features such as a recording or stimulating electrode. Combined with these tools, the injectrode system could serve as a closed loop device, delivering drug only when needed, ultimately allowing for efficacious independent disease management for chronic disorders.

Thesis Supervisor: Michael J. Cima
Title: David H. Koch Professor of Engineering

Thesis Reader: Robert S. Langer
Title: David H. Koch Institute Professor

Acknowledgements

I would first like to acknowledge my thesis supervisor, Professor Cima, for giving me the opportunity to work in his lab and learn about the process of designing, building, and testing medical devices for clinical translation. I've learnt more than I can imagine through his recommendations and wisdom, and I'm eager to learn more in the upcoming years. Professor Langer, my thesis reader, has also been a tremendous source of advice and guidance throughout these studies.

From the lab I would like to foremost acknowledge Dr. Canan Dagdeviren, for constantly pushing me to improve, and for her invaluable insight and advice along this journey. This research would also not have been possible without the help of my labmates, Kevin Spencer and Carlos Nuñez Lopez. Lastly, I would like to thank my parents, family, and friends for supporting me throughout these years and continuing to do so in whatever endeavor I choose. Without their support I certainly would not be where I am today.

Table of Contents

Figure List

Introduction

The human brain has long been an object of fascination throughout civilizations. Early theories of its function were diverse: Aristotle believed it to be a cooling system for the blood, and Hippocrates considered it to be the seat of intelligence. However, it was not until the advent of modern scientific techniques that scientists were able to confirm or disprove these theories. Perhaps most important in revolutionizing our understanding of the human brain was Ramon y Cajal. He used new staining techniques of the late 19th century and made the first breakthroughs in the characterization of individual neurons, the building blocks of neural circuits. Since then, our understanding of the way the brain works has advanced tremendously, although a lot remains to be discovered, and our interpretation is ever changing.

The brain is the sole organ responsible for cognition, emotion, learning, and thought. It is what distinguishes us from mere biological machines. It is also the primary mediator of the central nervous system, coordinating the myriad of chemical networks between organs to maintain homeostasis. It does so through intricate interfacing with the endocrine, immune, and gastrointestinal systems of the body. For example, the hypothalamus is a primary component of the hormonal renin-angiotensin-aldosterone system (RAAS), which regulates blood pressure and fluid balance within the body.

Our understanding of internal brain systems has also progressed. Scientists have typically compartmentalized the distinct regions of the brain responsible for different functions based on anatomical location. However, research is increasingly pointing towards a revision of this model,

with distinct neural networks being the functional building blocks of brain function. The dysychrony of these networks is hypothesized to be the cause of many neurological disorders [1].

In this thesis, I describe a device we developed for precise targeting of pathologic neural circuits, through local drug delivery and deep brain stimulation. To better elucidate its place in the current clinical landscape for neurological treatments, I will go over some of the problems with current treatments, using Parkinson's disease as the primary example.

Neuropsychiatric disorders

The complexity of the brain, and the diversity of innervations to other organ systems leaves many opportunities and ways for neural disorders to arise. The Brain Foundation lists over 60 disorders, and estimates that approximately 1 billion people suffer from neurological disorders worldwide [2]. A subclass of these diseases is neuropsychiatric disorders: mental disorders with biological underlying causes. Examples include Parkinson's (PD), Alzheimer's, schizophrenia, epilepsy, and mental health disorders. 1 in 4 American adults suffer from diagnosed mental disorder, with total costs of $317 billion per year. 5.4 million Americans have diagnosed Alzheimer's, while the ADI estimates the cost of Alzheimer's worldwide to be 1% of world GDP (604 billion) [3]. Parkinson's disease (PD) affects over 6 million people worldwide, and is estimated to cost >$25 billion/year in the US alone [4]. These disorders cost a fortune to treat continuously, and their incidence is only increasing in a growing elderly population. These diseases are part of a trend where healthcare costs are increasingly being spent of chronic disorders. According to the CDC, >66% of healthcare costs in the US are spent on treatment of chronic illnesses affecting 95% of older Americans [5].

These chronic conditions often lack effective treatments, and require expensive continuous monitoring and care with repeated hospital visits as a result. With the advent of personalized medicine, many resources are being devoted to develop techniques for independent chronic disease management. Many neuropsychiatric disorders arise due to a loss in synchrony in specific neural networks. Treatment of these diseases only requires specific targeting of the neural networks at the point of malfunction. However, most of neurological treatments lack the specificity to target these circuits appropriately. To elucidate this, I give the example of Parkinson's disease, arguably the most in-depth studied of this group of diseases. In the context of neuropsychiatric disease, a readily available closed-loop therapeutic addressing malfunctioning neural network nodes would have great potential in improving the quality of life for patients, as well as shrinking the burgeoning healthcare costs associated with them.

Parkinson's Disease symptoms and pathophysiology

Parkinson's disease (PD) is a neurodegenerative disorder that affects approximately 1% of the global elderly population [6]. It is a debilitating disorder that renders sufferers increasingly helpless throughout its progression, first causing uncontrollable motor symptoms such as bradykinesia and tremor, and finally resulting in dementia and psychosis. Because of this wide range of effects, effective treatment plans that adequately manage disease progression are limited and extremely costly. This incapacitates patients and resigns them to years of increasing helplessness in looking after themselves, and reliance on care providers to provide at best, partially symptom-relieving care. It is estimated that the total direct and indirect costs of PD are more than $25 billion per year in the US alone[4].

Pathologically, PD is identified by a loss in the dopamine (DA) neurons of the substantia nigra pars compacta (SNc). The SNc is one of the constituents of the basal ganglia (BG), a collection of subcortical nuclei that are heavily connected to the cortex, thalamus, and brainstem. The BG is instrumental in a number of processes including voluntary motor movements, cognition, emotion, and learning[7]. The loss of the BG DA feedback loop shown in figure 1 leads to dysregulation of thalamic output to the motor cortex, which in turn results in the hallmark motor symptoms of bradykinesia, rigidity, and tremor. Pre-symptomatically, PD pathology is also seen in the medulla oblongata, pontine tegmentum, and olfactory bulb. Therefore, the onset of PD may first be noticed from discrete symptoms such as a reduced sense of smell, a change in handwriting, and reduced facial expressions [8].

Another pathological finding in PD-afflicted brains is the presence of Lewy bodies, which consist primarily of α-synuclein; a common hypothesis is that a faulty ubiquitin-proteasome system (UPS) leads to excess aggregation of proteins that form Lewy bodies. Abnormal protein folding leads to an increase in ROS and free radicals, causing neural toxicity. SNc neurons are believed to be particularly susceptible to oxidative damage, which explains their pronounced loss, and the subsequent symptoms associated with insufficient DA within neural circuits. Given our incomplete knowledge about the pathophysiology, a PD diagnosis is essentially a clinical one [9, 10].

Other non-motor symptoms arise as the disease progresses: depression develops in almost 40% of cases, while Dementia typically develops 10 years following the onset of motor symptoms, with a pathology that is strikingly similar to that of Alzheimer's. Eventually, psychosis

eventually develops in 30% of cases, due to the loss of DA projections from the SNc to the mesolimbic system [10].

While some common genetic abnormalities have been identified among a minority (15%) of PD patients, no pervasive mutation has been found. It is believed that the predisposition to PD is driven by a specific interplay between genetic and environmental factors [11]. Evidence from PD research and treatment has led to its classification as a network disorder [12, 13]. Decreased DA destabilizes a few key neural circuits which leads to downstream large scale de-synchronization of multiple neural loops, and widespread consequent effects including inhibition of cognition and voluntary motor movement [1].

Current Treatments for PD

The various facets of PD and its symptoms make it a particularly difficult disease to treat. Current treatment standards at best decrease the severity of motor symptoms, allowing patients to lead a relatively normal life for a period of time. However, the efficacy of these treatments markedly decreases over time, and eventually the side effects outweigh the benefits. Treatments to date have focused on correcting the DA feedback loop within the BG, which is the cause of the debilitating motor symptoms of PD, and can be grouped into 2 categories: systemic drug administration and deep brain stimulation (DBS).

Systemic drug administration: L-DOPA (trade name levodopa) is the most commonly administered drug treatment for PD [14]. L-DOPA is a neurotransmitter precursor that is converted into dopamine by DOPA decarboxylase once it enters the central nervous system

(CNS). However, oral administration does not provide control over spatial or temporal resolution of DA levels in the target regions of the CNS. This then leads to increasing tissue resistance, necessitating administration of higher doses, which then causes DA toxicity to otherwise healthy neural circuits. With time, a host of severe motor side effects occur that, ironically, mimic PD pathology of DA feedback malfunction - these include levodopa-induced dyskinesia (LID) and DA dysregulation syndrome [14]. Other drugs also delivered systemically include dopamine agonists and MAO-B inhibitors, which inhibit the metabolism of DA. However none of these are as effective than levodopa [10].

Deep Brain Stimulation: A set of electrodes (~2mm in diameter) are inserted into the subthalamic nucleus (STN) and connected to a subcutaneously implanted pulse generator placed intraclavicularly. The electrodes are then stimulated periodically at high frequency (100-130 Hz). This acts as a 'reset' button on abnormal current/voltage oscillations within basal ganglia circuitry, and alleviates motor symptoms for some time after stimulation [15]. In particular, parkinsonian tremor is correlated with neural beta oscillations. These are 13-35 Hz oscillations originating in the striatum, detected overwhelmingly in the BG of PD patients and animal models using cyclic voltammetry [16]. It is likely that these oscillations are caused by the loss in synchrony that results from a decrease in DA feedback form the SNc to the striatum [17]. These beta band oscillations are attenuated following DBS of the STN [18-20]. However, while DBS show dramatic results in symptom reduction, the level of expertise and technology needed to maintain proper treatment regimens is formidable, which greatly limits the scale on which reliable DBS can be delivered. There is some debate about the mechanism of action of DBS, and

whether it reduces or increases STN activity [21]. Due to the complex interplay of STN loops within the BG, this has not yet been proved one way or another.

Treatment Limitations

Implanting rigid probes into the brain and tethering them to the skull often results in micromotion, as a result of the relative movement between the brain and skull. This micromotion can lead to consistent inflammation and glial scar formation around the probe, causing neuron migration away from the probe tip and less effective stimulation. Other hardware-complications such as battery failures, short circuits, and connection breakages can also lead to DBS probes fail [22].

Systemic drug dosing and DBS are therapeutics used for a variety of other diseases, including depression and epilepsy. The problems with these treatments are the same in all applications: lack of specificity. Drugs delivered systemically fail to address the key circuit deficiencies that cause these disorders. Similarly, bulky DBS probes stimulate indiscriminately and constantly, without regard for circuit function at the time. Over time, this leads to resistance to therapy, migration of neurons away from the probes. DBS also fails due to hardware-complications, and glial scarring as a result of micromotion. In PD, treatments seek to rectify PD by correcting the original DA circuit, but lack the spatiotemporal specificity to do so without causing a host of side-effects.

Neural drug delivery strategies

A variety of ongoing research seeks to address the issues described above and improve neural therapeutics. Over the past decade various new probe designs have been reported. These probes can contain electrodes for recording/stimulating, lumens for drug infusion, or both. Rigid probes typically suffer from the mechanical property mismatch with the relatively soft surrounding neural tissue. This leads to scarring and neural migration away from the tip, lowering the quality of electrical neural recordings, and necessitating the infusion of larger drug volumes to target surrounding tissue. One design that seeks to avoid this is flexible probes, which are implanted with a rigid guide needle. This flexibility decreases inflammation and scaring associated with micromotion and mechanical mismatch. Another approach is to make smaller probes, reducing the footprint, and thus subsequent inflammation. Silicon micromachining is often used to this end [23]. However, it is often difficult for long (>2cm) microfabricated probes to be stiff enough to be inserted without a guide needle, which increases trauma and possibly damages the surrounding tissue. Varying probe shapes can also improve durability. One group found that a flexible sinusoidal probe resulted in less glial scar formation around it, resulting in more stable neuronal recordings over time [24].

For drug infusion, convection-enhanced delivery (CED) probes rely on passive diffusion over a longer period of time [25]. Other microfluidic channels have been combined with electrodes for combined therapy [26-32]. These were either connected to upstream pumps *ex vivo* or. However all these probes achieve certain requirements while failing in others. While they are sufficiently long to target any area of rodent brains, most are not long enough to penetrate past the cortex in large primates, limiting their targeting abilities to intracortical regions [33]. For example, the

NeuroMedicator device consists of an implanted probe as well as discrete drug reservoirs which can be opened on demand [34]. However, it is only 8mm long. This is particularly significant as most pathology in neuropsychatric disease occurs in the midbran or deep brain. A few deep brain probes have been developed for simulatenous electrical recording and drug delivery, however the only pumping mechanism used is *ex vivo*, limiting their use to research tools, and not clinical therapeutics [35]. *Ex vivo* pump connections allow for a wide variety of high pressure pumping mechanisms[36, 37], but are obviously impractical for use in chronic disease management. Another probe developed with multiple lumens, allowing for multi-drug delivery, suffers from both these problems as well, it is only 7mm long, and relies on purely *ex vivo* pump connections [38].

In vivo implantable pump development is another field in which a lot of developments have been reported in the literature. The compromise is one between pumping pressure, battery life, durability, biocompatibility, and size. Different pumping mechanisms exist, largely classified as either passive and active. Passive pumping is essentially diffusion-driven, but limited by some physical factor such as a semipermeable membrane or high resistance microchannel. Active pumping required energy input, and can use mechanical, chemical, or electrostatic mechanisms to achieve output. Piezoelectric pumps are often used when high pumping pressure is not required, as they are reliable, acheive high flow rates, and can be finely tuned [39]. An example an application of this is the piezoelectric micropump developed as a closed loop therapeutic for diabetes [40]. Magnetic field actuating mechanisms are attractive in that they can be applied externally, without the need for extra device implantation [41]. Electrical actuation has also been

implemented successfully in applications such as chronic cancer drug therapy, allowing for wireless control. However dispensing pressures are low [42].

Fine control is required for drug delivery to the brain, where small volumes need to be delivered over a short period of time. Such controlled on-demand delivery of small amounts requires an active, responsive, high-performance pump. The only pumping mechanism able to satisfy this is mechanical actuation.

The Injectrode

Our device, which we term the 'injectrode' combines electrical (DBS) and chemical delivery with an unprecedented level of control and feedback, allowing for intelligent, effective treatment. It is made up of a stainless steel outer shell, containing an electrode and two glass lumens with inner diameter of 20μm. The electrode allows for stimulation or recording, while drug is infused through each of the glass lumens. Each of the glass lumens connect to stainless steel connectors leading to implantable iPrecio micropumps. The iPrecio SMP-300 micropump is a wirelessly-controlled, commercially available peristaltic pump. We chose this pump due to be able to infuse across the extremely high fluidic resistances created by the thin glass lumens. The entire injectrode system is shown in figure 2.

SMP-300 Micropump

The SMP-300 micropump is a commercially available implantable pump for slow programmed drug delivery in small animals. It is also wirelessly controllable, allowing for manipulation and programmed infusions once implanted. We have repurposed this pump in combining it with the injectrode device for acute nanodosing of specific brain regions.

The pumps works on the basis of peristalsis. A rotating CAM pushes pins up in a peristaltic wave, compressing the compliant tubing and resulting in fluid outflow (figure 3). There are 4 pins, each deployed once per full CAM rotation. One full CAM rotation results in 3.4μl of fluid ejected.

Methods

Device Fabrication

Two glass lumens (20μm ID, Vitrocom) and a Tungsten electrode (FHC) are placed on a microfabricated polyimide template, and inserted into a 31G Hamilton needle. Once inside, epoxy is flushed and cured between the needle and lumens. This device is connected to the micropump using PEEK tubing, stainless steel connectors, and UV cured medical grade epoxy. This process is shown in figure 4.

Device characterization

An iPrecio SMP-300 micropump (Primetech Corp., Japan) is obtained, and the original external Styrene-ethylenebutylene-styrene (SEBS) tubing cut, leaving only the first 25mm of outlet tubing. This was done to avoid stretching of the compliant SEBS tubing when used in conjunction with high fluidic resistances. A stainless steel connector is inserted into the pump fluid outlet and into the PEEK tubing, connecting the two. The junction is glued using UV light curable silicone adhesive (Loctite 5055, Henkel Corporation, Rocky Hill, CT. USA), creating a water-tight secure junction.

The injectrode is placed into a custom-made PTFE (polytetrafluoroethylene) holder attached to a syringe pump to be used as a vertical frame (Harvard Apparatus PHD 2000). The assembly is combined with a computer controllable Mettler Toledo microbalance for pump characterization experiments.

A plastic weighing dish is half-filled with de-ionized water (~30μl) and placed on the weighing plate in the microbalance. The glass cap of the microbalance is removed and parafilm is stretched taught over the top. A circular hole is cut out in the center of the parafilm using scissors. The injectrode is lowered through the hole and the pump set to infuse fluid until a drop of fluid appears at the top of the injectrode. At this point, the device is further lowered such that the tip of the injectrode is submerged within the water in the weighing dish. 20μl of mineral oil (paraffin oil and liquid petrolatum, Mallinckrodt Chemicals, Dublin, Ireland) is then placed on top of the water in the weighing dish, minimizing evaporation of water. The system is allowed to stabilize before any infusions are tested. The pump is programmed wirelessly using proprietary iPrecio pump software. This setup is depicted in figure 4.

The microbalance is set to output a reading 2 times per second to a computer using an RS232 serial connector. Commercially-available Advanced Serial Data Logger software (AGG Software) is used to acquire the data and export it to Microsoft Excel for further Analysis. For every infusion, data recording begins and ends at least 10 minutes before and after infusion onset and end, respectively.

Device *in vivo* biocompatibility assessment.

F344 (SAS Fischer) rats were purchased from Charles River laboratories and maintained under standard 12 hour light/dark cycles.

Surgeries

3 rats underwent bilateral craniotomy and had an injectrode device implanted on the left side of the cortex and a ground screw implanted on the right hand side. The screw was placed such that tip did no penetrate the brain. Briefly, the animals were placed in a stereotactic frame, and a midline incision made to expose the skull. 2 burr holes were created using a dental drill. The left hand side burr hole was created using a 1mm drill bit (Meisinger GmbH, Germany), for injectrode implantation, while the right hand side burr hole was made using a 0.5mm drill bit, for insertion of the ground reference screw also used for structural support of the implant. The injectrode was implanted approximately 5mm posterior to the bregma and 2mm lateral to the midline, while the ground screw was inserted 5mm posterior to the bregma and 2.5mm lateral to the midline. The injectrode and screw were then inserted, cemented to the skull using C&B Metabond adhesive (Parkell Inc., Edgewood NY) and Orthojet dental cement (Lange Dental, Wheeling, IL USA), and the incision was closed using 5-0 monofilament non-resorbable suture. Animals displaying extensive post-operative morbidity more than 72 hours post-surgery were euthanized and not further used in the study.

At 56 days post-implantation, the animals were euthanized using Carbon Dioxide asphyxiation. Each animal consequently underwent cardiac perfusion of 60ml 1x Phosphate Buffered Saline (PBS) solution (Corning Inc., Corning, NY, USA), followed by 60ml 4% Paraformaldehyde

(PFA) solution (Alfa Aesar, Ward Hill, MA). The head was then removed and immersed in 4% PFA for 48 hours. The implanted devices were extracted, and the brain removed and placed in 4% PFA overnight, and consequently in sinking solutions of increasing sucrose (Amresco Inc., Solon, OH, USA) concentration (10%, 20%, 30%, overnight or until brain sinks). All animal protocols were approved by the MIT Committee for Animal Care.

Histology

The brain was embedded in frozen tissue embedding medium (Sakura Finetek USA, Torrance, CA), and frozen in a liquid nitrogen bath. 20μm transverse slices were cut using a Leica CM1900 cryostat (Leica Biosystems Inc., Buffalo Grove, USA), starting at the top of the brain, and descending 80mm, past the tips of the previously implanted devices. Slides were stored at -80 °C.

Slides were stained for astrocytes (Glial fibrillary acidic protein (GFAP)), microglia (Iba1), neurons (NeuN), and nuclei (Hochst/DAPI) removed from -80 °C, placed at room temperature for 20 minutes, and rehydrated by placing in a 1xPBS solution for 10 minutes. Samples were then immersed in blocking solution (5% Bovine Serum Albumin (BSA) (Rockland, Limerick, PA)) for 50 minutes, followed by overnight incubation at 4 °C in primary antibody incubation solution. (1:100 mouse anti-GFAPx488 Alexafluor, 1:300 rabbit anti-NeuN, (EMD Millipore, Billerica, MA, USA), 1:300 goat anti-Iba1 (Abcam, Cambridge, MA, USA) in incubation buffer (1% BSA, 1% normal Dk serum, 0.3% Triton X-100, 0.1% Sodium Azide).

Slides were rinsed 3 times in 1x PBS (0.1% Tween), and incubated in secondary antibody

solution (1:300 Dk x Gt x Cy3 & 1:300 Dk x Rb x Dy650 (Abcam) for 40 minutes. Samples were rinsed 3 times in 1x PBS, and incubated with Hochst solution (0.1μg/ml) for 5 minutes, followed by mounting in gold antifade mounting medium (Life Technologies, Carlsbad, CA USA)

Data Analysis

All images were taken using fluorescence microscopy (EVOS FL Auto, Life Technologies, Grand Island, NY), and analyzed with custom MATLAB scripts kindly provided by Dr. Jeffrey Capadona of Case Western Reserve University. These scripts define the boundary of the hole created by the injectrode implantation, and then sum the intensity of each of the 4 stains in 2mm radial increments from the hole boundary, up to 1100mm away from the edge of the hole. For the purposes of data analysis, GFAP intensities were used as the primary indicator for the extent of glial scar formation around the implant. The intensities were then averaged into 50mm bins, and normalized such that the intensity 900-1100μm away was equal to 1. This was done for 4 pictures for each animal, which were averaged to create a GFAP intensity vs. distance profile. The profiles for each of the 3 animals were then combined and averaged.

In vivo device characterization using Positron Emission Tomography (PET):

Radioactive Cu64 was obtained from the Mallinckrodt Institute of Radiology (St. Louis, MO) in the form of Copper Chloride, and diluted with saline to 2μCi/μl activity concentration. Cu64 solution was then infused intracerebrally into F344 Fischer Rats (Charles River Laboratories) using each of the following 3 methods:

(1) A 10μl luer lock syringe (#1701 Hamilton, Reno, NV) was connected to a 31G needle and pre-loaded with 5ml of Cu64 solution. A 1mm burr hole was created in an untreated animal under isofluorane anesthesia 5mm posterior to the bregma and 2mm lateral from the midline. The needle was lowered stereotaxically through the burr hole, 8mm into the brain. 2μl of Cu64 was delivered using a Stoelting Quintessential Stereotaxic Injector, at a rate of 0.2μl/min for 10 minutes. The needle was left in place for 5 minutes post end-infusion before being retracted slowly. The burr hole was then covered with bone wax and the cranial incision sutured with 5-0 non-resorbable monofilament suture.

(2) Animals with an implanted injectrode probe were anesthetized with isofluorane. One of the fluidic outputs of the device was connected to the same syringe/needle set up previously described in case 1. 1.67μl of Cu64 was delivered at a rate of 10μl/hr for 10minutes. The needle was immediately disconnected from the device post-infusion.

(3) Animals with an implanted injectrode probe were anesthetized with isofluorane. This time, one of the fluidic outputs of the injectrode was connected to an iPrecio micropump. 1.67μl of Cu64 was delivered at a rate of 10μl/hr for 10minutes.

Immediately following incision suture (case 1) or infusion (cases 2 &3), the anesthesized animal was imaged using a Perkin Elmer G8 PET /CT Preclinical Scanner for six 10 minute frames over the course of an hour. Images are reconstructed using MLEM 3D with 60 iterations.

Only PET could be performed on the entire animal, due to the size of the bore and gantry. Thus, animal from case (1) was euthanized using CO_2 asphyxiation and decapitated. The head was then imaged with PET and CT for a single 10minute frame. Co-registration is then done with the original PET Data that was obtained *in vivo* and the PET/CT data that was obtained Ex-vivo.

Results

Device Characterization

The iPrecio micropumps are manufactured connected to Styrene-ethylenebutylene-styrene (SEBS) tubing. We initially tested the pumps by connecting this tubing to the injectrode lumens, these infusion profiles are shown in figure 6. As seen, fluid output continues even significantly after the programmed end of infusion. This effect is exacerbated in higher flow rates; flow rates of 10μl/hr yielded significantly longer infusions than did 8μl/hr flow rate infusions. We hypothesize that this was due to the relatively high compliance of the SEBS tubing and high resistance of the lumens.

To model this compliance effect, we assume the model of a syringe pump pushing fluid through a high compliance tube and high resistance lumen in series, shown below:

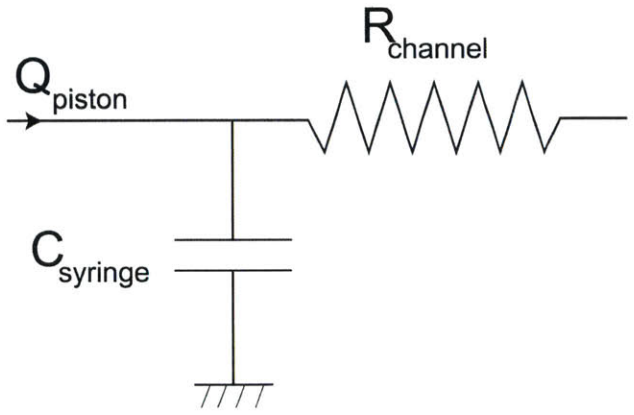

The fluidic resistance of a vessel is given by:

$$R_{channel} = \frac{8\mu L}{\pi r^4}$$

Where: R is the resistance of the channel

μ is the viscosity of the fluid

L is the length of the channel

r is the radius of the channel

Using node analysis, we predict that a step change in input flow would then yield a flow equation of

$$Q_{piston} = \frac{1}{R_v}\Delta P + \frac{C_V d\Delta P}{dt}$$

where the flow development to its asymptotic value is characterized by a time constant of

$$\tau = R_v C_V = \frac{8\mu l}{\pi r^4} VK$$

where: V is the total volume

K is the effective compressibility of the system

$R_{channel}$ is composed of 2 resistances here, that of the SEBS tubing and the glass lumen. However, as the inner diameter of the glass is substantially smaller than that of the SEBS tubing (20μm compared with 550μm), and the resistance increases exponentially with decreasing diameter, we neglect the resistance of the tubing. Similarly, we neglect the compliance of the glass as its Young's modulus is very large compared to that of the tubing.

Applying the following values for the variables:

$$\mu = 10^{-3} \text{ Pa.s}$$

$$L = 10\text{cm}$$

$$r = 10\mu\text{m}$$

We obtain ➔ $R = 2.57\text{x } 10^{16}$ N.s/m^5

The pressure required to pump against resistance is dependent on flow rate:

$$P = QR$$

For the 2 cases tested here, we obtain:

Q = 10µl/hr ➔ P = 70.8 kPa

Q = 8µl/hr ➔ P = 57.16 kPa

Both of these pressures are an order of magnitude above the pump's pressure rating of 0 to 7.8kPa. As a result of both these confounding factors, we take a closer look at the compliant behavior.

Taking the derivative of the graphs in figure 6, we get Flow rate vs. Time plots shown in figure 7. There is a sharp increase in flow rate at the onset of infusion, followed by a gradual decay post end-infusion. Ideally, flow rate would drop to zero once infusion ends. Instead, we see a decay, in line with the compliance model described above. High-pressure infusion leads to compliance build up in the tubing, which is gradually released once the infusing pressure stops. Isolating the decaying portion of the graphs, we can fit the data to a single term exponential model, derived from the model described above.

The model fit takes the form of

$$Y = ae^{-\lambda t}$$

Such that $\tau = \frac{1}{\lambda}$

Both graphs were fit to this single term exponential model shown in ***figure 8.*** The best fit equations found were:

$$Y = 15.56e^{-0.0175t}$$

$$Y = 69.05e^{-0.01987t}$$

The consistency of the time constants under both conditions give merit to the hypothesis that the compliance of the tubing is greatly affecting the system's infusion performance.

To overcome this, we replaced the PE tubing with high-pressure PEEK tubing, commonly used in high pressure HPLC systems. We used stainless steel connectors for the interface of the PEEK tubing and pump output. We tested this set up with both long and short injectrode devices, with 3 infusion protocols each:

1) 10 minute infusion with flow rate 10μl/hr
2) 10 minute infusion with flow rate 1μl/hr
3) 10 minute infusion with flow rate 0.1μl/hr

These infusions profiles are shown in figure 9. We measured the compliance of the decay in flow rate post end-infusion for the 10min infusion at 10μl/hr through the long injectrode, to compare with the initial infusions done with SEBS tubing. The decay is shown in figure 10, and the exponential found is

$$Y = 1714e^{-0.33t}$$

$$Y = 1714e^{-0.33t}$$

The time constant here is decreased by an order of magnitude, indicating a significantly faster drop in flow rate at end-infusion, which indicates substantially less compliance buildup during the infusion.

Table 1 below quantifies the performance of the iPrecio micropumps in each of these cases with % volume and time overinfusion.

Table 1. Pump % overinfusion through long and short probes

Short Probe				
		Programmed Infusion (μl)	*Actual Infusion (μl)*	*% Over infusion*
10min	0.1μl/hr	16.7	33	97.60
	1μl/hr	167	221	32.34
	10μl/hr	1667	1613	-3.24
Long Probe				
		Programmed Infusion (μl)	*Actual Infusion (μl)*	*% Over infusion*
10min	0.1μl/hr	16.7	31	85.63
	1μl/hr	167	388	132.34
	10μl/hr	1667	2131	27.83

After noticing the overinfusion for even the small infusion, we decided to test the variation of compliance-induced variability to infusion flow rate. We tested 2 alternates in addition to 1μl/hr 10min protocol, all with identical total end volume theoretically infused:

1. 1min at 10μl/hr
2. 2min at 5μl/hr
3. 10min infusion at 1μ /hr

These infusions are shown in figure 11. Similar flow rate decay profile analyses were conducted, and we found that the effective compliance of the system increased noticeably with higher flow rates. This is shown graphically in figure 12. The percent over-infusion is tabulated in table 2.

$$Y = 1392e^{-1.211t}$$

$$Y = 261.8e^{-0.5191t}$$

$$Y = 5.72e12e^{-8.386t}$$

Table 2. Overinfusion for equivalent protocols through short probe

Short Probe			
	Programmed Infusion(μl)	*Actual Infusion(μl)*	*% Over infusion*
1μl/hr 10min	167	221	32.34
5μl/hr 2min	167	269	61.08
10μl/hr 1min	167	373	123.35

In vivo biocompatibility assessment

The injectrode system is meant for long-term chronic implantation. To validate the system's biocompatibility, we implanted the injectrode over a period of 8 weeks and stained brain histology for typical glial markers. We chose to quantify the distribution of GFAP, an astrocyte stain, as it is the most commonly used marker of neural inflammation. Figure 13 shows representative microscope images of the different fluorescent stains, as well as the binned GFAP intensity results as a function of distance from the edge of the implant.

In vivo device characterization using PET

In vivo infusions and consequent live animal imaging was performed to confirm functionality of the device once implanted. As described in the Methods section, 3 different protocols were performed and imaged. In cases 2 and 3, the cross sectional profile of the drug bolus delivered was measured over time, these results are shown in figure 15 and 16.

1. Acute syringe infusion (shown in in figure 14)

   The bolus of delivered drug is clearly seen, as well as the backflow that results from withdrawal of the needle post-infusion.
2. Microsyringe pump infusion through implanted Injectrode device (shown in in figure 15)
3. iPrecio micropump infusion through implanted injectrode device (shown in in figure 16)

Discussion

There is a lack of technologies available for precise, repeated targeting of small deep brain structures. This presents a problem not only in benchside neuroscience research, but especially in clinical treatments to neurological disease. Many of these disorders are being uncovered as a loss in synchronization of neural circuitry, with the problem often originating in a particular faulty region. The gold standard of treatments for these disorders is systemic drug dosing, which lacks the spatiotemporal resolution to target the faulty region in isolation, resulting in collateral damage as it affects other healthy neural tissue as well. This presents a problem of drug delivery. To address this problem, we developed and tested the injectrode system, a multichannel implantable probe connected to implanted micropumps for acute, controlled drug delivery.

The SMP-300 micropumps we used are wirelessly programmable, allowing us to program them once implanted. We first characterized the performance of the pumps when connected to extremely high fluidic resistances, beyond their max rating of 7.8kPa. We connected the pump to both short and long versions of the injectrode probe, 1cm and 10cm long. The short version is used for rodent studies, whereas the larger probe is intended for primate and eventually human implantation. Our first infusion results indicated that the stock SEBS tubing connected to the pump is highly compliant in the face of these high resistances, resulting in fluid outflow over a long period of time, significantly beyond the programmed end of infusion. In the case of a 10 minute infusion at 10μl/hr, fluid continuously flowed out of the injectrode for 10 hours, albeit at a decaying rate (figure 6). We modeled the flow as that through a capacitor-resistor circuit, and examined the flow rate decay profiles. The decay time constant fit was consistent across both

infusion profiles tested, supporting our logic that the compliant tubing was the cause of the long over-infusion.

Such gradual delivery is exactly what we aimed to improve upon with our device, and so we switched to low-compliance high pressure PEEK tubing. We tested this setup with both the long and short probes, and showed much more consistent infusion profiles across different infusion protocols. The pumps performed well even when faced with high resistances, and in almost all cases over-infused beyond the theoretical programmed volume to be delivered. The drop in flow rate at the end of programmed infusion as now much more abrupt, and applying the capacitor-resistor model to this data gave time decay constants an order of magnitude higher than previously found.

We were pleased with our finding that the pumps were able to pump consistently and repeatedly at pressures much higher than their commercial ratings, with no leakage. However, a limitation of the pump came as a result of its mechanism of action. The peristaltic motion of the pistons inherently relies on the deformation of compliant tubing within the pump, creating a source of compliance during infusion that could not be avoided.

After characterizing the performance of the device *in vitro*, we shifted to studying the pump's behavior *in vivo*. We implanted the small probes in rodents for 8 weeks for chronic biocompatibility studies. Fluorescent microsopy showed a thin ring of astrocytes (GFAP) surround the implant. This scar formation is the normal reaction, and is seen for any neural implant. The thin size of this scar here was reassuring, and alleviated our original concern that a

thick scar formation might impede fluid outflow. Furthermore, neurons and microglia were seen in healthy numbers located around the implant, indicating that no toxicity is caused by the implant to the surrounding tissue (figure 13).

We used PET imaging to support our *in vitro* infusion characterization, and to show that the device could be used to infuse small volumes of drug locally. Figure 14 shows the problem with current neuroscience techniques, whereby significant backflow exists when acutely inserting a needle through a skull burr hole to infuse a drug or viral vector. No such backflow exists when infusing through the implanted injectrode probe (figures 15, 16). We infused 1.67μl of radioactive Cu-64 over 10 minutes using either a syringe pump or the iPrecio micropumps previously characterized *in vitro*. In both cases, boluses of fluid where seen at the end of the device within the brain, 1-2 mm in diameter (figure 15,16). This is expected as 1.67 μl corresponds to $1.67mm^3$ in volume. Assuming a spherical shape for the drug delivered, the diameter of such a sphere would be 1.5mm. When large molecules are infused into the brain, their distribution is often limited to the intracranial space between brain tissue, due to a lack of permeability of the blood-brain barrier. However, as a small ion, copper can readily cross this barrier and is internalized by the cells. By imaging the infusion over time, we show that the bolus delivered remains at the point of delivery, with no significant diffusion occurring over the course of an hour post infusion. Intensity line profiles shown in figure 15 confirm that the bolus is steady over time. This highlights the device's strengths in local targeting of specific brain regions, preventing unwanted delivery to other regions.

Conclusion and Future Directions

The injectrode system holds great promise as a new standard of care in the treatment of neuropsychiatric disorders. We have shown the system's functionality in on-demand local drug delivery to deep brain regions, something that has never before been reported using a completely implanted system. The design of the probe also allows for 2 separate infusion lumens for the simultaneous infusion of 2 different drugs. One lumen could theoretically be used as a washout drug, to counteract the effect of the other, or as a separate, complementary drug. No model for this was studied here, as these studied focus more on device characterization and functionality *in vitro* and *in vivo*, but this characteristic is a powerful tool to have at hand. A single lumen implanted probe would require the original drug be flushed out before any other drug can be infused. This could be extremely dangerous if some toxicity or unwanted side-effects arise from the original drug.

Another aspect of the device that has not been explored is the electrical recording and stimulating. The probe design also incorporates an electrode in conjunction with the 2 fluidic lumens. The stimulating electrode could be used as a complementary treatment strategy to drug delivery, much like L-DOPA and DBS in the treatment of Parkinson's disease. On the other hand a recording electrode could be used to detect abnormalities in neural oscillations, and be used as an indicator for the need for the acute delivery of drug. In this way one can envision the design of a complete closed loop feedback system using the injectrode system. Such a system will allow for independent disease management of chronic conditions, a huge improvement over the current standard of care, which would result in lower healthcare costs associated with chronic disease treatment, and a higher quality of life for patients suffering from these debilitating diseases.

Figures

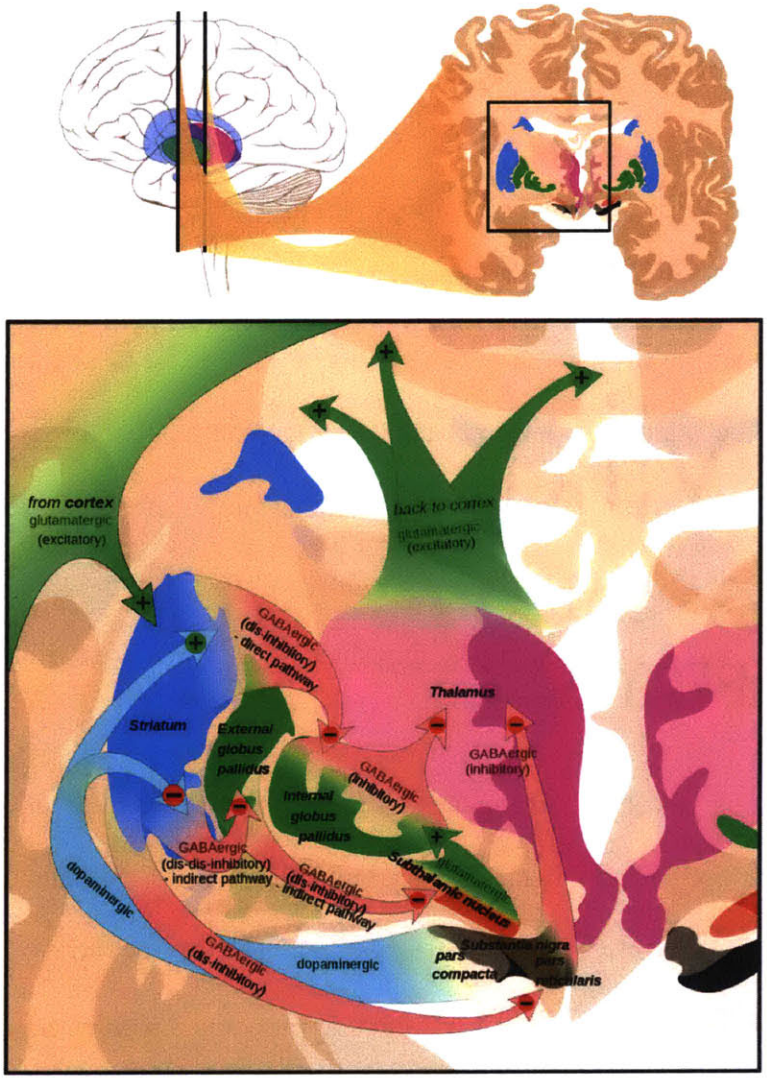

Figure 1. Schematic of circuitry of the basal ganglia. In Parkinson's disease, the dopamine feedback loop from the SNc to the Striatum is lost.

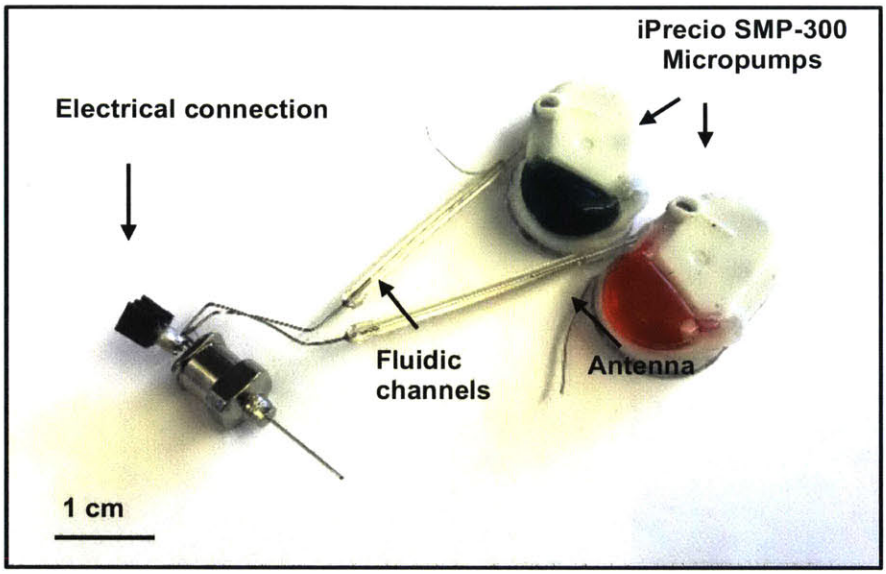

Figure 2. **The Injectrode device connected to iPrecio micropumps.** Each channel is connected to a single pump. The probe also contains an electrode, the electrical connection to which is also shown.

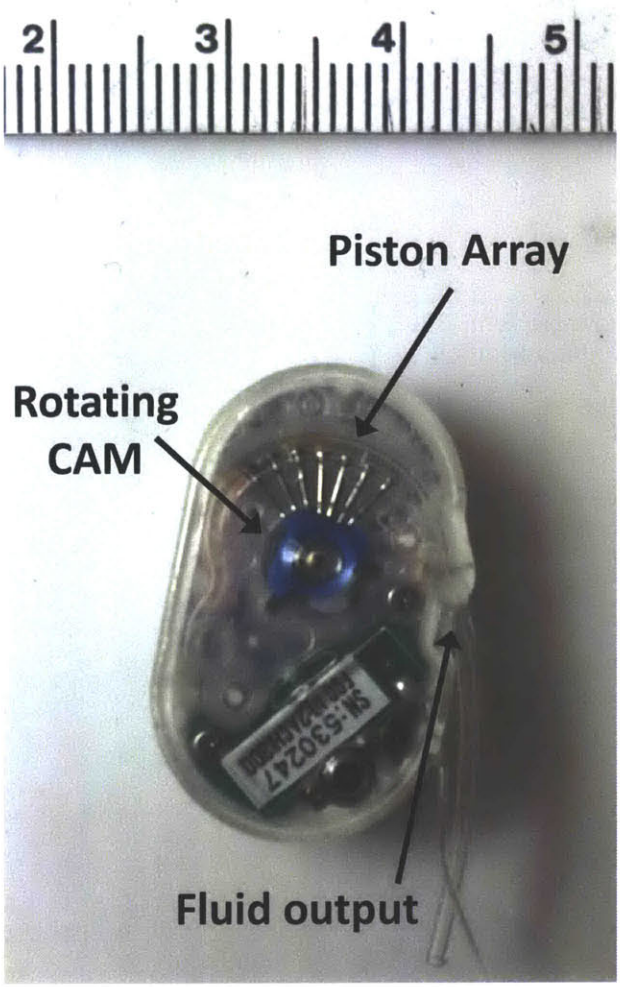

Figure 3. iPrecio micropump pumping mechanism. The CAM rotates clockwise, resulting in a peristaltic wave of pistons pushing against the compliant tubing containing the fluid.

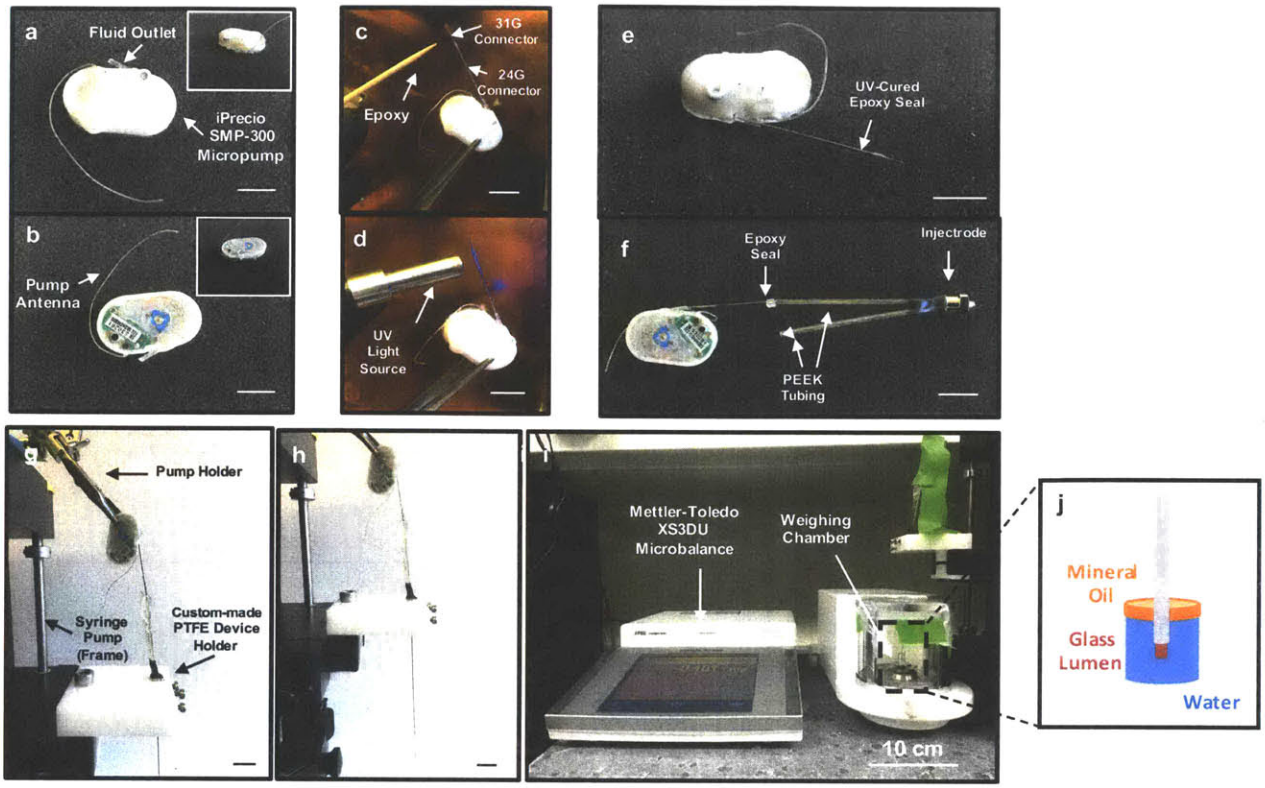

Figure 4. Device assembly and characterization protocol. Top (a) and Bottom (b) views of an iPrecio SMP-300 micropump. The original external tubing cut, leaving only the first 2.5mm of outlet tubing. (Right inset figures of (a) and (b) show isometric views of top and bottom of the SMP-300 micropump, respectively). (c) A 24G stainless steel connector is inserted into the pump fluid outlet, and a 31G connector placed within the larger connector. (d) The 2 are glued together using UV light curable epoxy, creating a water-tight a secure junction (e). (f) The protruding end of the 31G connector is inserted into the PEEK tubing of the injectrode device, and the junction glued using the same UV light curable epoxy. (g,h) The injectrode is placed into a custom-made PTFE (polytetrafluoroethylene) holder attachable to a syringe pump to be used as a vertical frame (Harvard Apparatus PHD 2000), and (i) the assembly combined with a Mettler Toledo microbalance for pump characterization experiments, with sensitivity set to 1μg. A thin film of mineral oil is then placed on top of the water to prevent evaporation from interfering with the recorded weights. (j) illustrates the distinct layers of water and oil in the weighing dish, and relative position of the injectrode tip. All scale bars are 1cm long, unless otherwise noted.

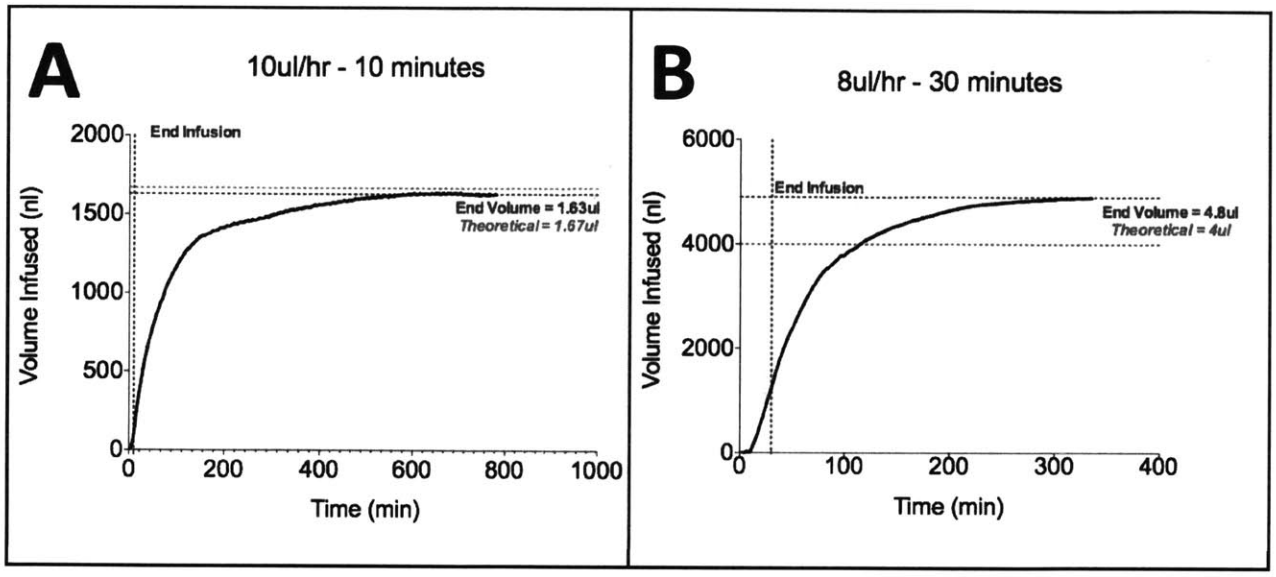

Figure 5. Compliant Tube infusion profiles

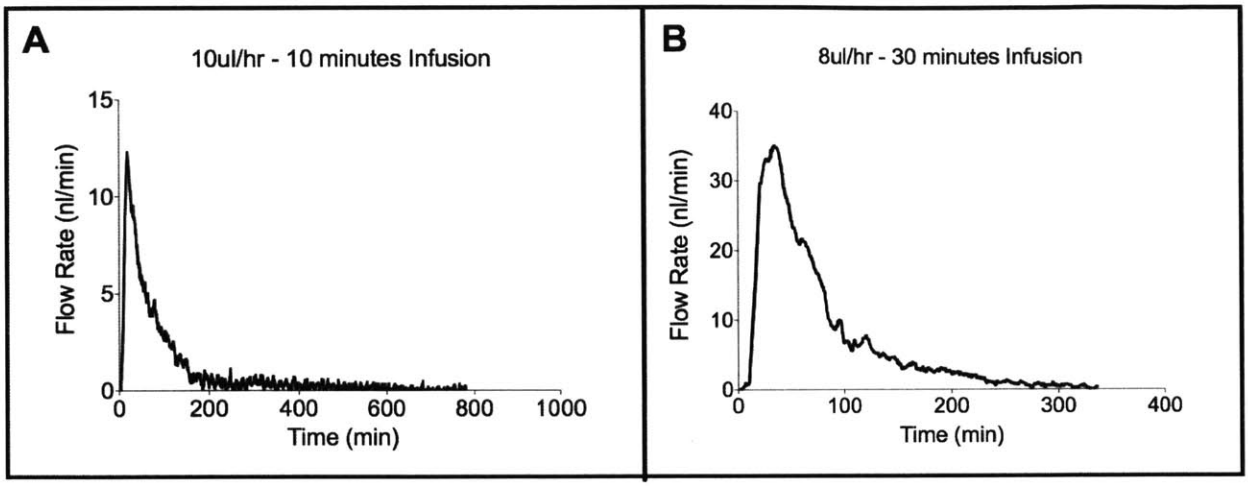

Figure 6. Compliant tube Flow Rate vs. Time, obtained as the derivatives of the infusion plots.

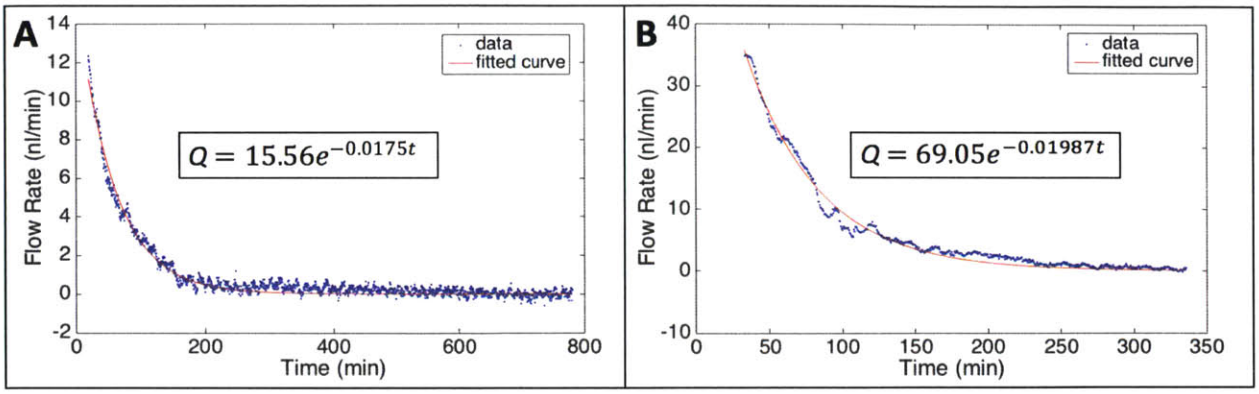

Figure 7. Compliant tubing model fit for infusions shown in figure 6. (A) corresponds to a 10 minute infusion at 10μl/hr while (B) corresponds to a 30 minute infusion at 8 μl/hr.

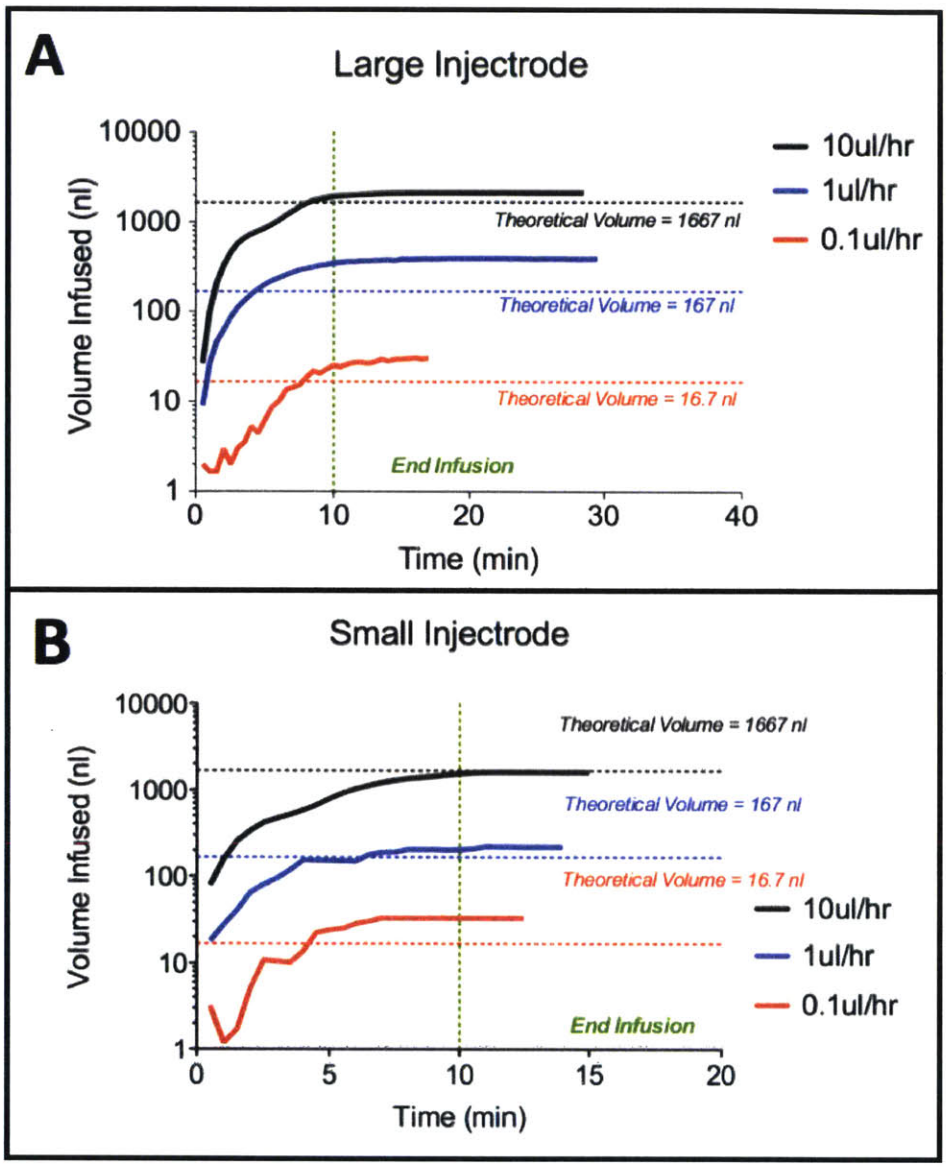

Figure 8. PEEK tubing infusion profiles. These were done using both large and small injectrode probes.

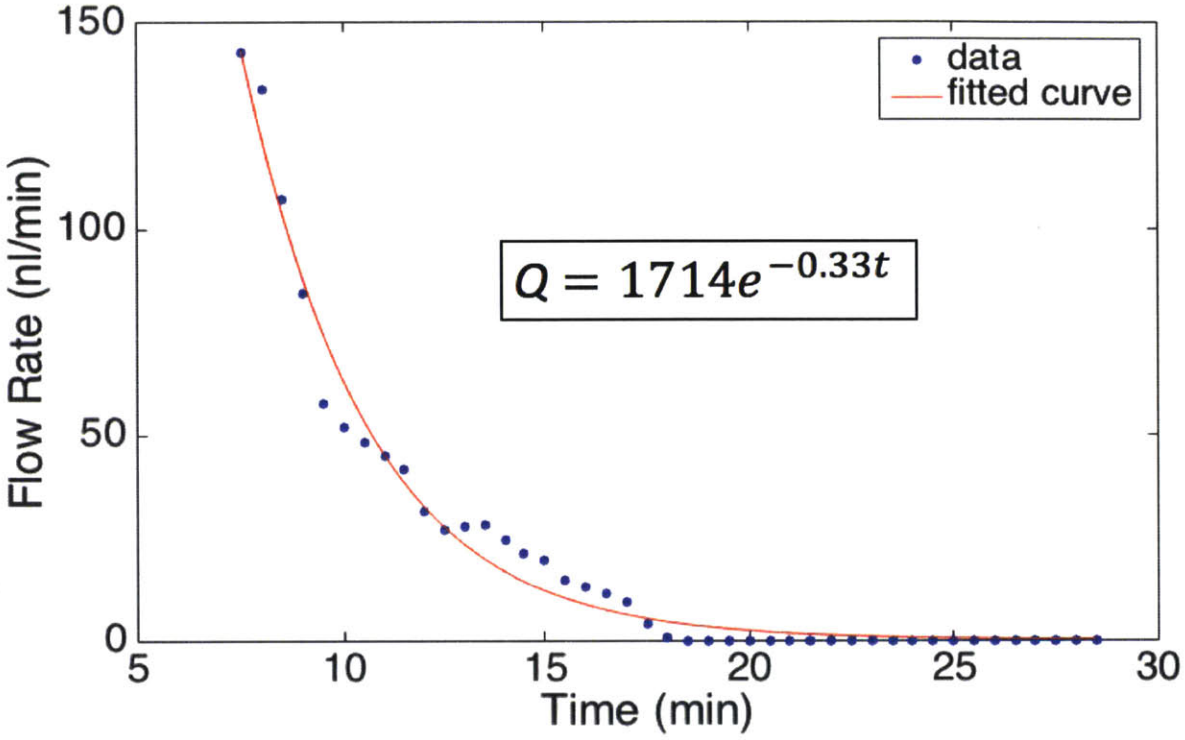

Figure 9. PEEK Tubing infusion flow rate, for the 10 minute infusion at 10 μl/hr, through the large injectode device. Graph was obtained by taking the derivative of the corresponding profile in figure 8. This infusion profile is identical to that done in compliant tubing, shown in figure 8A and 9A.

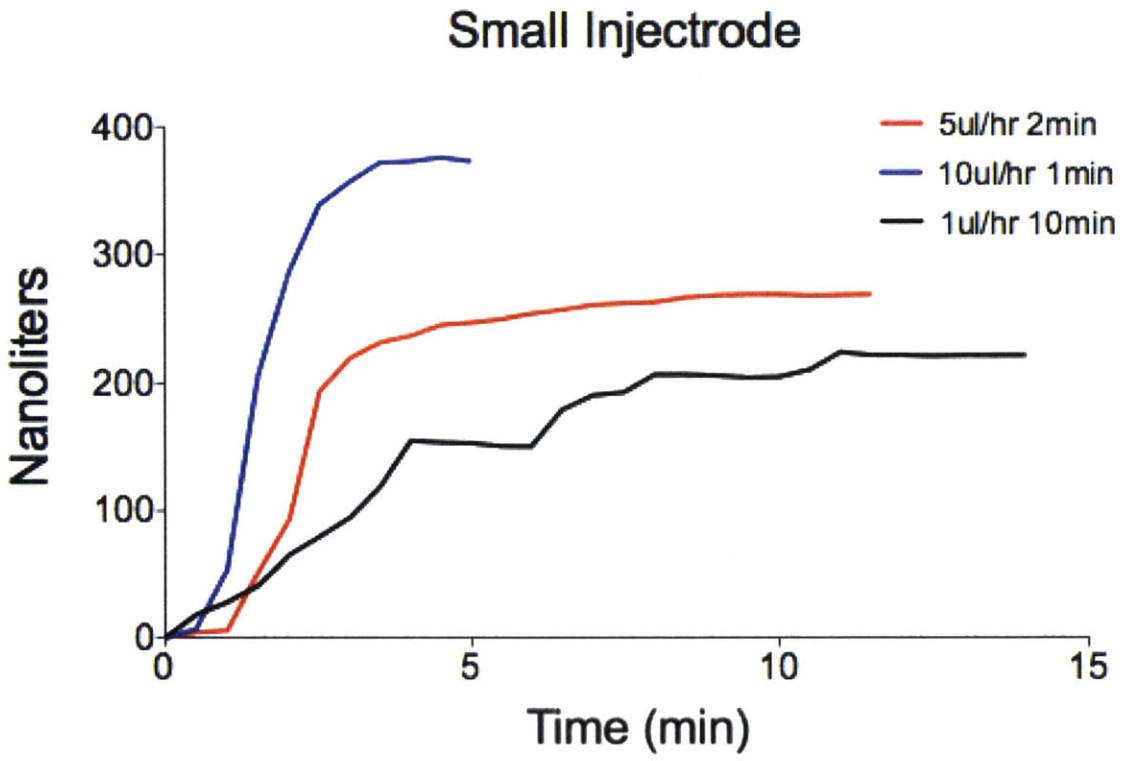

Figure 10. Alternate Infusion protocols using PEEK tubing.

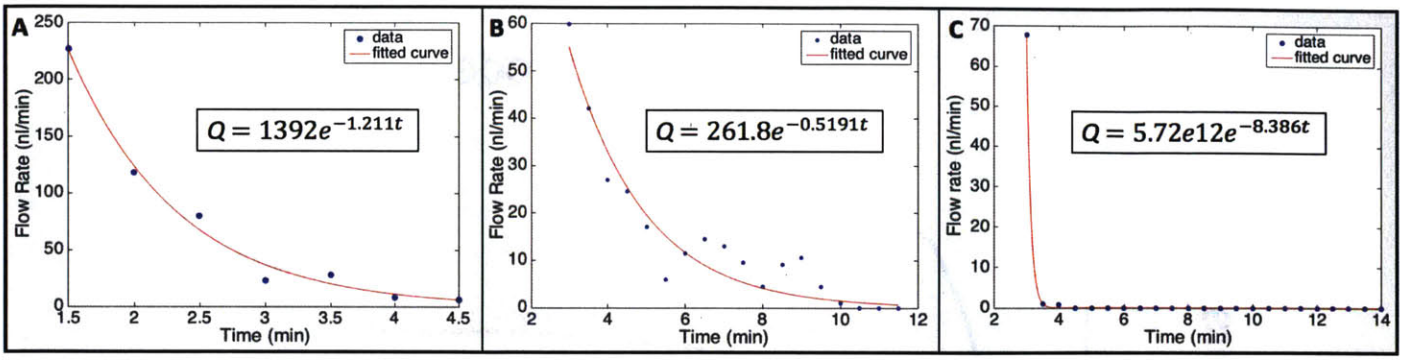

Figure 11. Infusion Flow Rate vs. Time plots for the infusion profiles shown in figure 10. (A) corresponds to 1 minute infusion at 10 μl/hr, (B) corresponds to a 2minute infusion at 5 μl/hr , and (C) corresponds to a 10minute infusion at 1 μl/hr.

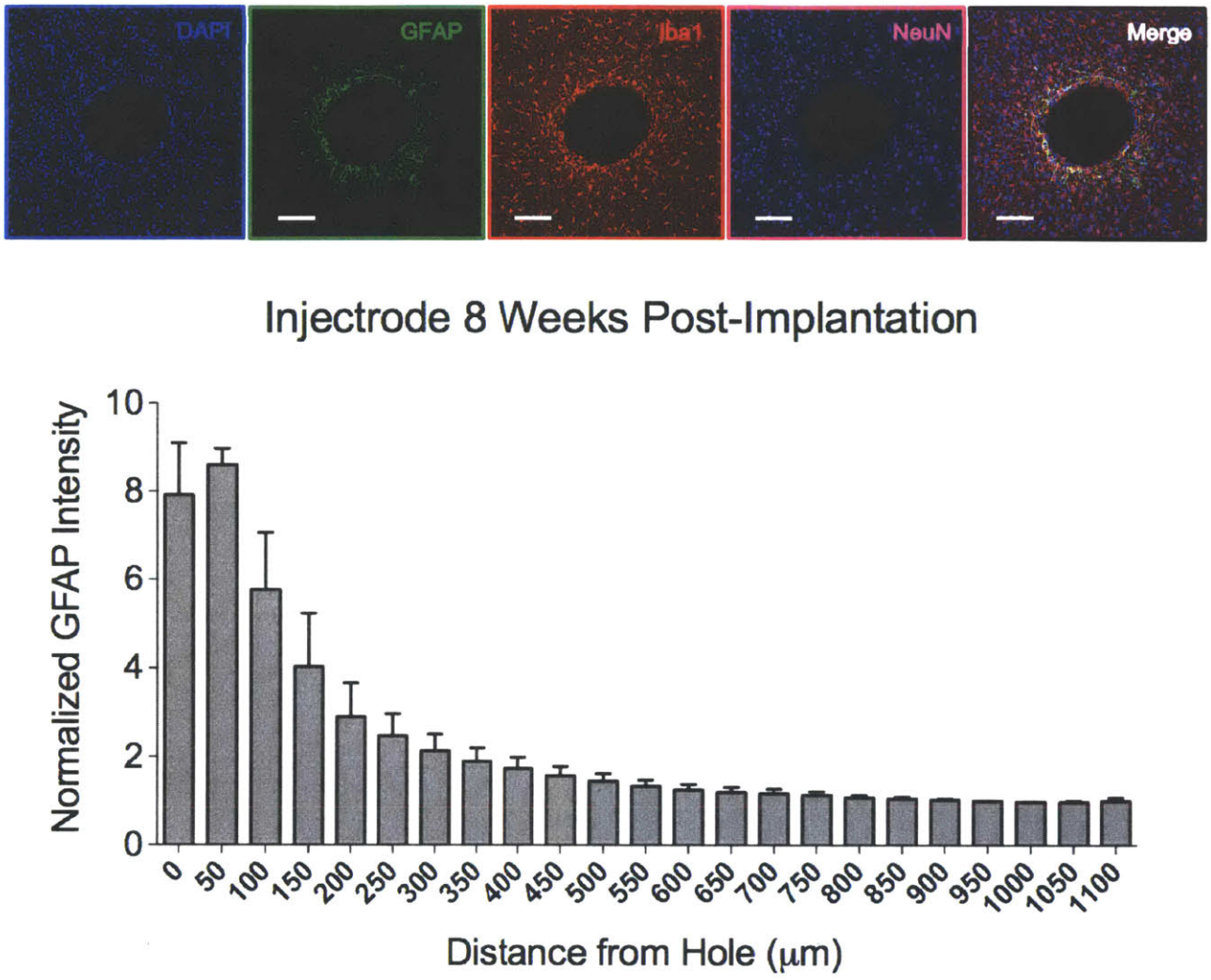

Figure 12. 8 week biocompatibility study stains. (Top) Representative confocal fluorescence Images of horizontal brain slices showing stab wounds created by implanted injectrode devices, 8 weeks post-implantation. These show immune histochemical staining for DNA (DAPI, blue), Astrocytes (GFAP, green), activated microglia (Iba1), and neurons (NeuN). All histological and confocal settings were kept consistent across groups. Image contrast uniformly enhanced using ImageJ for visibility, such that 0.1% of pixels are saturated. Scale bars 100 μm.

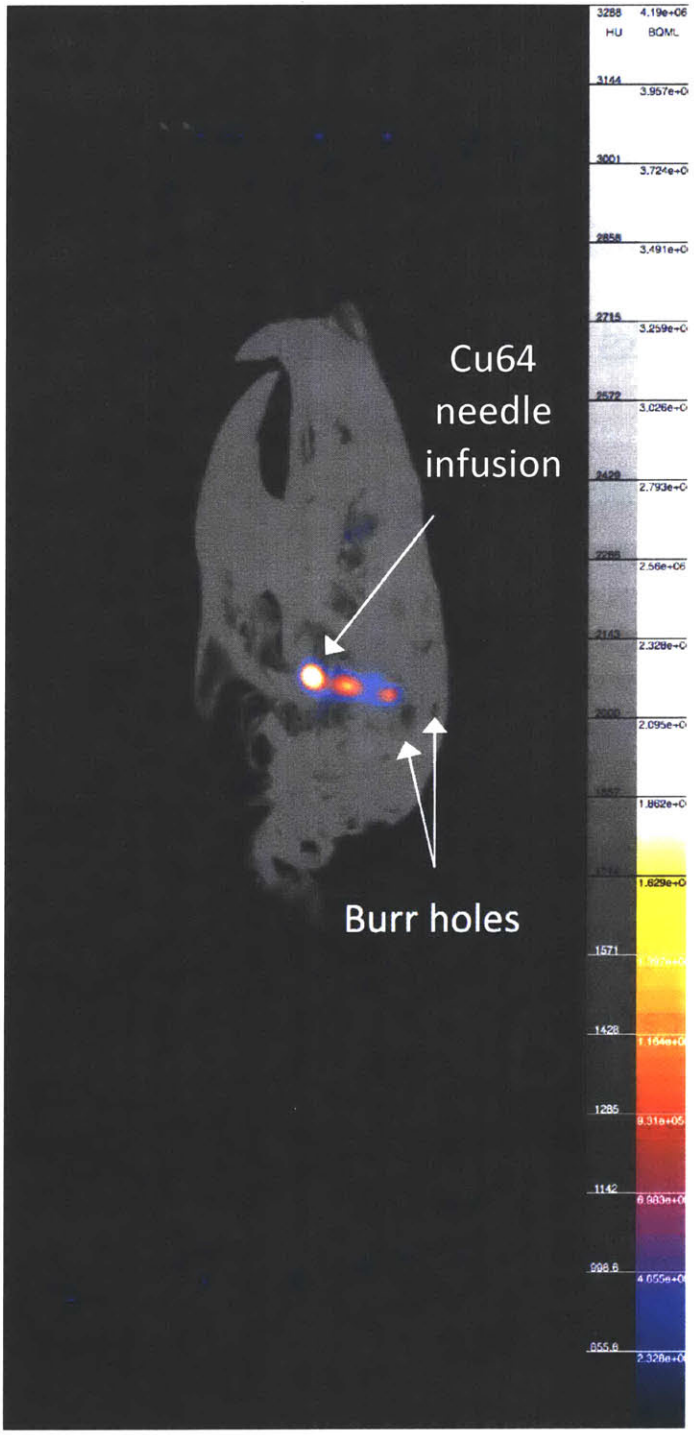

Figure 13. PET and CT Imaging post-Acute Infusion using a inserted needle. Needle is removed post-infusion.

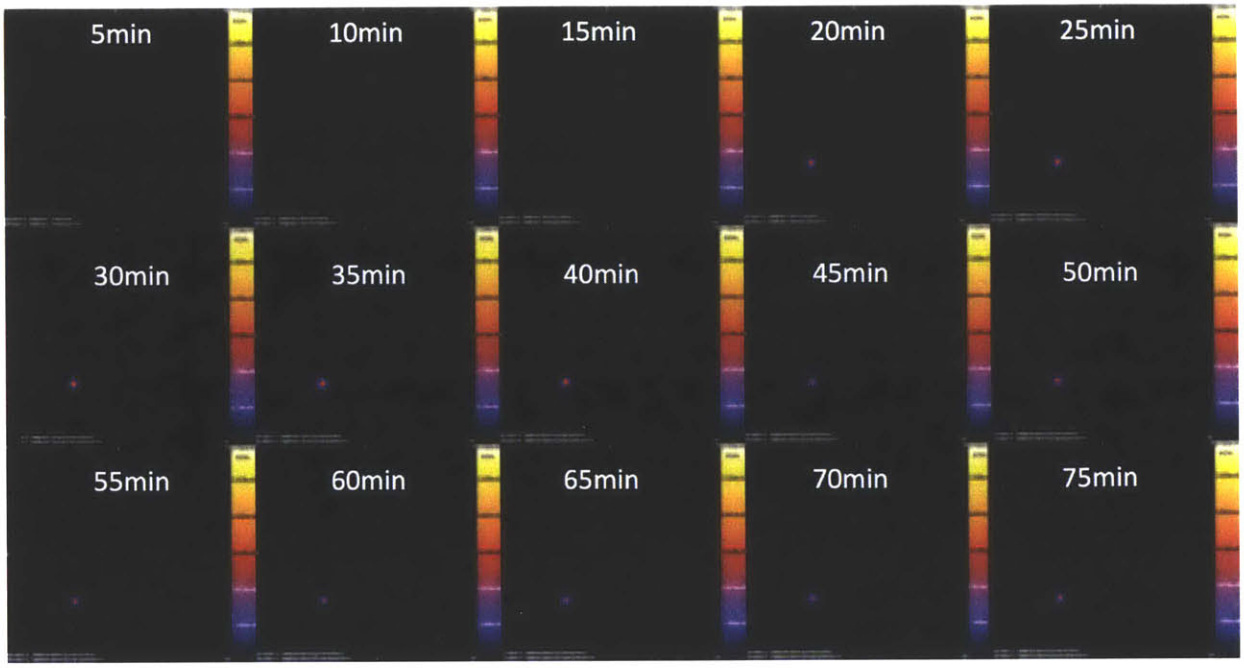

Figure 14. PET Imaging post syringe infusion. Imaging started simultaneously with 10 minute infusion. Infusion ended at 10 minutes.

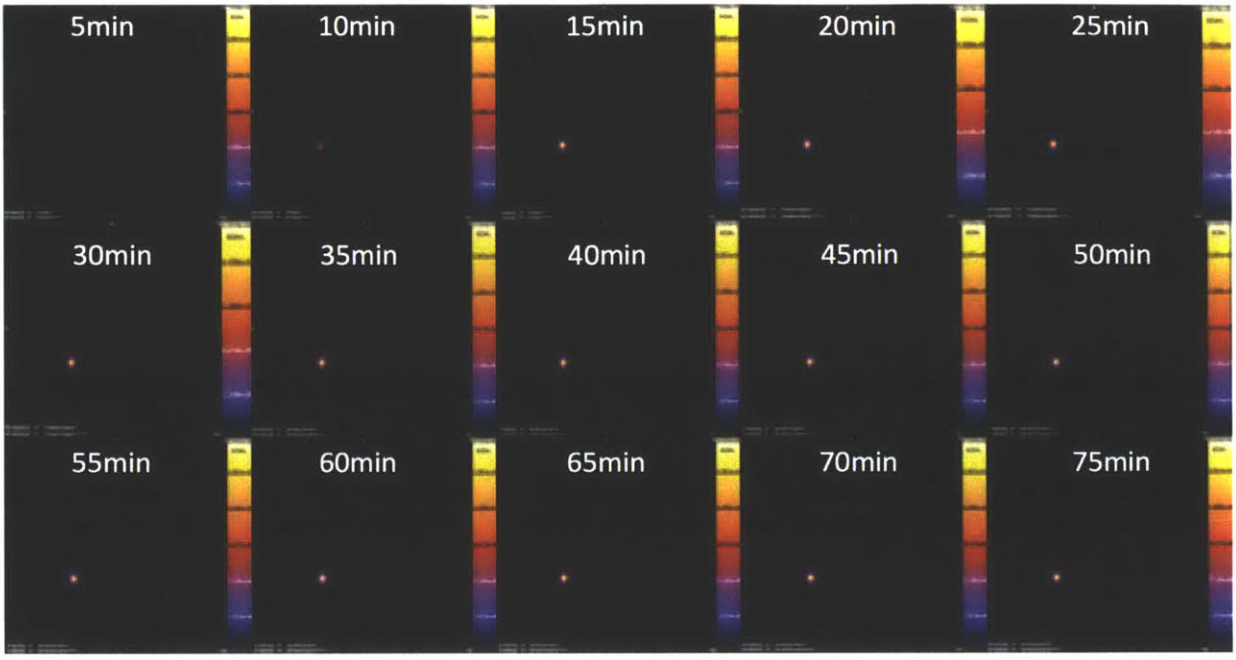

Figure 15. PET Imaging post micropump infusion. Imaging started simultaneously with 10 minute infusion. Infusion ended at 10 minutes.

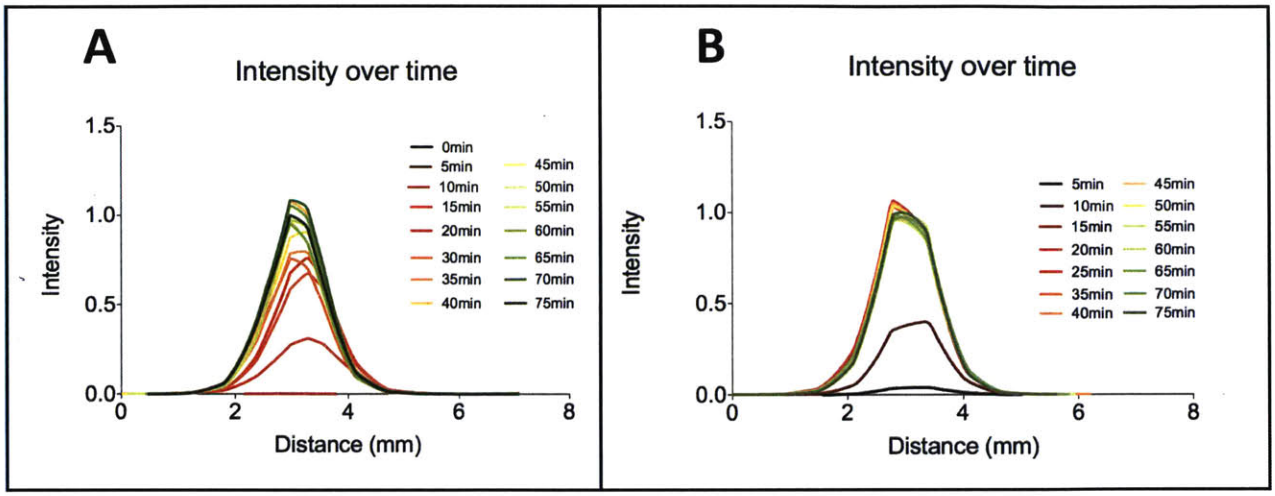

Figure 16. Intensity line profiles across center of bolus seen in transverse plane from PET results. (A) Corresponds to the infusion using a syringe pump, shown in figure 14, while (B) corresponds to the infusion using the micropump, shown in figure 15.

References

[1] P. J. Uhlhaas and W. Singer, "Neural synchrony in brain disorders: relevance for cognitive dysfunctions and pathophysiology," *Neuron,* vol. 52, pp. 155-68, Oct 5 2006.

[2] U. N. Centre. (2007, March 20, 2016). *Nearly 1 in 6 of world's population suffer from neurological disorders*. Available: http://www.un.org/apps/news/story.asp?newsid=21689&cr=neurological -.VvBZ76grLEY)

[3] M. I. f. B. Research. (2014, March 20, 2016). *Brain Disorders: By the Numbers*. Available: https://mcgovern.mit.edu/brain-disorders/by-the-numbers#PD

[4] P. s. D. Foundation. (2014). *Statistics on Parkinson's*. Available: http://www.pdf.org/en/parkinson_statistics

[5] C. f. D. C. a. Prevention, "The state of Aging and health in America 2013," U. D. o. H. a. H. Services, Ed., ed. Atlanta, GA, 2013.

[6] H. Shafique, A. Blagrove, A. Chung, and R. Logendrarajah, "Causes of Parkinson's disease: Literature Review," *Journal of Parkinsonism and Restless Legs Syndrome,* vol. 1, pp. 5-7, 2011.

[7] S. Grillner and B. Robertson, "The basal ganglia downstream control of brainstem motor centres-an evolutionarily conserved strategy," *Curr Opin Neurobiol,* vol. 33C, pp. 47-52, Feb 12 2015.

[8] H. Braak, J. R. Bohl, C. M. Muller, U. Rub, R. A. de Vos, and K. Del Tredici, "Stanley Fahn Lecture 2005: The staging procedure for the inclusion body pathology associated

with sporadic Parkinson's disease reconsidered," *Mov Disord,* vol. 21, pp. 2042-51, Dec 2006.

[9] K. K. Chung, Y. Zhang, K. L. Lim, Y. Tanaka, H. Huang, J. Gao, *et al.*, "Parkin ubiquitinates the alpha-synuclein-interacting protein, synphilin-1: implications for Lewy-body formation in Parkinson disease," *Nat Med,* vol. 7, pp. 1144-50, Oct 2001.

[10] C. A. Davie, "A review of Parkinson's disease," *Br Med Bull,* vol. 86, pp. 109-27, 2008.

[11] T. T. Warner and A. H. Schapira, "Genetic and environmental factors in the cause of Parkinson's disease," *Ann Neurol,* vol. 53 Suppl 3, pp. S16-23; discussion S23-5, 2003.

[12] C. C. McIntyre and P. J. Hahn, "Network perspectives on the mechanisms of deep brain stimulation," *Neurobiol Dis,* vol. 38, pp. 329-37, Jun 2010.

[13] M. Trost, S. Su, P. Su, R. F. Yen, H. M. Tseng, A. Barnes, *et al.*, "Network modulation by the subthalamic nucleus in the treatment of Parkinson's disease," *Neuroimage,* vol. 31, pp. 301-7, May 15 2006.

[14] T. P. S. Group, "Levodopa and the Progression of Parkinson's Disease," *New England Journal of Medicine,* vol. 351, pp. 2498-2508, 2004.

[15] H. Bronte-Stewart, C. Barberini, M. M. Koop, B. C. Hill, J. M. Henderson, and B. Wingeier, "The STN beta-band profile in Parkinson's disease is stationary and shows prolonged attenuation after deep brain stimulation," *Exp Neurol,* vol. 215, pp. 20-8, Jan 2009.

[16] M. A. J. Michael L.A.V. Heien, R. Mark Wightman, "Resolving Neurotransmitters Detected by Fast-Scan Cyclic Voltammetry," *Anal. Chem.,* vol. 76, pp. 5697-5704, 2004.

[17] C. M.-K. M. M. McCarthya, X. Gub, E. S. Boyden, X. Hanb, and N. Kopella,, "Striatal origin of the pathologic beta oscillations in Parkinson's disease," *Proc Natl Acad Sci U S A,* vol. 108, 2010.

[18] G. C. McConnell, R. Q. So, J. D. Hilliard, P. Lopomo, and W. M. Grill, "Effective deep brain stimulation suppresses low-frequency network oscillations in the basal ganglia by regularizing neural firing patterns," *J Neurosci,* vol. 32, pp. 15657-68, Nov 7 2012.

[19] A. D. Dorval, G. S. Russo, T. Hashimoto, W. Xu, W. M. Grill, and J. L. Vitek, "Deep brain stimulation reduces neuronal entropy in the MPTP-primate model of Parkinson's disease," *J Neurophysiol,* vol. 100, pp. 2807-18, Nov 2008.

[20] A. D. Dorval and W. M. Grill, "Deep brain stimulation of the subthalamic nucleus reestablishes neuronal information transmission in the 6-OHDA rat model of parkinsonism," *J Neurophysiol,* vol. 111, pp. 1949-59, May 2014.

[21] M. M. M. Sabato Santaniello, Erwin B. Montgomery Jr., John T. Galed, Nancy Kopell, and Sridevi V. Sarmaa,, "Therapeutic mechanisms of high-frequency stimulation in Parkinson's disease and neural restoration via loop-based reinforcement," *Proc Natl Acad Sci U S A,* 2015.

[22] A. A. Michael Y. Oh, Seong H. Kim, Anthony E. Lang, Andres M. Lozano, "Long-term Hardware-related Complications of Deep Brain Stimulation," *Neurosurgery,* vol. 50, June 2002.

[23] H. J. Lee, Y. Son, D. Kim, Y. K. Kim, N. Choi, E.-S. Yoon, *et al.*, "A new thin silicon microneedle with an embedded microchannel for deep brain drug infusion," *Sensors and Actuators B: Chemical,* vol. 209, pp. 413-422, 2015.

[24] H. S. Sohal, A. Jackson, R. Jackson, G. J. Clowry, K. Vassilevski, A. O'Neill, *et al.*, "The sinusoidal probe: a new approach to improve electrode longevity," *Front Neuroeng,* vol. 7, p. 10, 2014.

[25] K. B. Neeves, C. T. Lo, C. P. Foley, W. M. Saltzman, and W. L. Olbricht, "Fabrication and characterization of microfluidic probes for convection enhanced drug delivery," *J Control Release,* vol. 111, pp. 252-62, Apr 10 2006.

[26] S. E. S. Demetrios P. Papaegeorgiou, Sanfor C. Bledsoe, Jr., Kensall D. Wise, "A Shuttered Neural Probe With On-Chip Flowmeters for Chronic In Vivo Drug Delivery," *Journal of Microelectromechanical Systems,* vol. 15, August 2006.

[27] A. Altuna, E. Bellistri, E. Cid, P. Aivar, B. Gal, J. Berganzo, *et al.*, "SU-8 based microprobes for simultaneous neural depth recording and drug delivery in the brain," *Lab Chip,* vol. 13, pp. 1422-30, Apr 7 2013.

[28] J. John, Y. Li, J. Zhang, J. A. Loeb, and Y. Xu, "Microfabrication of 3D neural probes with combined electrical and chemical interfaces," *Journal of Micromechanics and Microengineering,* vol. 21, p. 105011, 2011.

[29] S. Spieth, O. Brett, K. Seidl, A. A. A. Aarts, M. A. Erismis, S. Herwik, *et al.*, "A floating 3D silicon microprobe array for neural drug delivery compatible with electrical recording," *Journal of Micromechanics and Microengineering,* vol. 21, p. 125001, 2011.

[30] K. L. S. Scott T. Retterer, Christopher S. Bjornsson, Keith B. Neeves, Andrew J. H. Spence, James N. Turner, William Shain, Michael S. Isaacson, "Model Neural Prostheses With Integrated Microfluidics- A Potential Intervention Strategy for Controlling Reactive Cell and Tissue Responses," *IEEE Transactions on Biomedical Engineering,* vol. 51, November 2004.

[31] K. Gao, G. Li, L. Liao, J. Cheng, J. Zhao, and Y. Xu, "Fabrication of flexible microelectrode arrays integrated with microfluidic channels for stable neural interfaces," *Sensors and Actuators A: Physical,* vol. 197, pp. 9-14, 2013.

[32] P. Rohatgi, N. B. Langhals, D. R. Kipke, and P. G. Patil, "In vivo performance of a microelectrode neural probe with integrated drug delivery," *Neurosurg Focus,* vol. 27, p. E8, Jul 2009.

[33] S. Spieth, A. Schumacher, F. Trenkle, O. Brett, K. Seidl, S. Herwik, *et al.*, "Approaches for drug delivery with intracortical probes," *Biomed Tech (Berl),* vol. 59, pp. 291-303, Aug 2014.

[34] S. Spieth, A. Schumacher, C. Kallenbach, S. Messner, and R. Zengerle, "The NeuroMedicator—a micropump integrated with silicon microprobes for drug delivery in neural research," *Journal of Micromechanics and Microengineering,* vol. 22, p. 065020, 2012.

[35] A. Pongrácz, Z. Fekete, G. Márton, Z. Bérces, I. Ulbert, and P. Fürjes, "Deep-brain silicon multielectrodes for simultaneous in vivo neural recording and drug delivery," *Sensors and Actuators B: Chemical,* vol. 189, pp. 97-105, 2013.

[36] Y. Liu, L. Chen, and L. Sun, "Design and Fabrication of a MEMS Flow Sensor and Its Application in Precise Liquid Dispensing," *Sensors (Basel),* vol. 9, pp. 4138-50, 2009.

[37] J. N. Bin Wang, Yoav Litvin, Donald W. Plaff, Qiao Lin, "A Microfluidic Approach to Pulsatile Delivery of Drugs for Neurobiological Studies," *Journal of Microelectromechanical Systems,* vol. 21, February 2012.

[38] H. Shin, H. J. Lee, U. Chae, H. Kim, J. Kim, N. Choi, *et al.*, "Neural probes with multi-drug delivery capability," *Lab Chip,* vol. 15, pp. 3730-7, Sep 21 2015.

[39] A. T. Evans, Srinivas Chiavuri, and Yogesh B. Gianchandani, "A Multidrug Delivery System Using a Piezoelectrically Actuated Silicon Valve Manifold With Embedded Sensors," *Journal of Microelectromechanical Systems,* vol. 20, pp 231-238, 2011

[40] G. Liu, C. Shen, Z. Yang, X. Cai, and H. Zhang, "A disposable piezoelectric micropump with high performance for closed-loop insulin therapy system," *Sensors and Actuators A: Physical,* vol. 163, pp. 291-296, 2010.

[41] S. Rahimi, E. H. Sarraf, G. K. Wong, and K. Takahata, "Implantable drug delivery device using frequency-controlled wireless hydrogel microvalves," *Biomed Microdevices,* vol. 13, pp. 267-77, Apr 2011.

[42] M. M. Teymoori and E. Abbaspour-Sani, "Design and simulation of a novel electrostatic peristaltic micromachined pump for drug delivery applications," *Sensors and Actuators A: Physical,* vol. 117, pp. 222-229, 2005.